ICAST2014 #007

Active vibration control systems with improved sound radiation properties

Thomas Haase[1*], Christian Schubert[1], Hans Peter Monner[1]

[1] Adaptronics, Institute of Composite Structures and Adaptronics, German aerospace center (DLR), Braunschweig, Germany

Abstract

In the field of feedforward active vibration control (AVC) of plate structures the local vibration reduction around the error sensors can have a negative impact on the sound radiation. Therefore, very often the active structural acoustic control (ASAC) approach is recommended to control the sound radiation of plate structures. Nevertheless, ASAC systems require a lot of error sensors to establish a fine sensor grid to estimate the radiated sound power due to radiation modes. The large error sensor number is very cost intensive and the estimation of the radiation modes for larger or more complex structures is quite difficult. Therefore the use of AVC is still the most common way to control the sound radiation of plates with feedforward controllers. In order to improve the ability of AVC systems to reduce sound radiation the presented paper addresses the optimal error sensor placement for a feedforward controller. The feedforward controller is used to reduce the flexural vibration at the accelerometers (error sensors) whereas the geometrical positions of these error sensors are optimized by a sound power cost function. The geometrical optimization of the error sensors leads to new controlled operational deflection shapes (ODS's) which have a different sound radiation behavior. Furthermore, the resulting ODS's of the active vibration control systems are analyzed in terms of global vibration, radiation efficiency and phase distributions. The simulations and the experiments are conducted on an aluminum plate of size 800mm x 600mm x 3mm which is mounted on its four corners. A broadband stochastic point force disturbance is applied due to a shaker.
It can be shown that the optimized sensor positions have a higher sound power reduction compared to the sensors placed with gramian observability and a comparable to an ASAC system. The simulated behavior is also verified by experimental investigations on the aluminum plate.

1. INTRODUCTION

In the last two decades, a lot of active vibration control (AVC) systems and active structural acoustic control (ASAC) systems have been designed to reduce the flexural vibration and the sound radiation of plate structures. In order to reduce the sound radiation, ASAC systems are known as superior than AVC systems[4]. By using, for example, the radiation modal expansion theory[11], a control system can directly influence the radiated sound power by post processing the surface velocities of the structure with the estimated radiation modes. In order to achieve a precise estimate of the radiated sound power a fine regular sensor grid has to be measured or an extended model of the plate has to be measured[20]. In the case of a feedforward controller the measurement of an extended model of the plate is not sufficient because the disturbance signals have to be known too. Thus large or complex structures require a high number of error sensors to establish the sensor grid causing higher costs. Furthermore, an ASAC system highly

*Thomas Haase, thomas.haase@dlr.de

reduces the radiated sound power of plate structures but it can also increase the flexural vibration of the structure in the frequency range of inefficient radiating structural modes[10]. Despite the drawbacks, in these cases AVC systems are still used most commonly for noise reduction[13].
In order to optimize feedforward control systems much has been done on actuator and sensor placement, e.g. see review papers[7, 12, 23]. There are mainly two options to optimize actuator and sensor locations. The first one is to use the eigenmodes of the structure to calculate modal observability or modal controllability or another observability/controllability metric[1, 12, 18]. Also the combination of observability/controllability metrics and an optimization algorithm is possible. The second one is to combine an optimization algorithm with the calculation of a specific control scheme for a given actuator and sensor configuration, for examples see[3, 26].
The first method allows lower costs in measurement and calculation, since there is only a structural model needed. With the structural model the observability/controllability metrics can be easily calculated. The second method is more complex because the control algorithm has to be calculated for each optimization step. In the case of a genetic optimization this step efforts a high computational cost. Nevertheless, with the second method a prediction of the system under control can be given and a detailed cost function for the control system can be determined[21,22]. In the thesis of Nijhuis[21] collocated sensor/actuator pairs and in Nijhuis and de Boer[22] non-collocated sensors and actuators are optimized with the second method described above and the radiated sound power is used as the cost function.
Also the optimization of a PVDF sensor position and a structural piezoceramic actuator position for sound power reduction is presented in the litrature[3]. These studies are optimizing decentralized feedback, single-input single-output (SISO) systems or sequentially optimized small multiple-input multiple output (MIMO) systems only. However, publications that study multiple structural sensors can be rarely found[17]. E.g. in publication[17] the electrical combination of structural sensors is focused only. Finally, only one combined sensor is used by the control system.
To the authors best knowledge very few studies are presented where multiple-input multiple-output AVC systems with structural sensors and actuators are optimized to reduce the radiated sound power. Furthermore, a detailed comparison between MIMO AVC systems and ASAC systems cannot be found. In consequence, there is still a lack of knowledge how AVC systems can be directly optimized such that they are able to reduce the sound radiation of plate structures. Therefore, this study investigates a MIMO AVC system with fixed actuators and sound power optimized structural error sensors and compares it to an ASAC system. The objectives of this study are:

- Optimization of multiple structural error sensors such that the sound radiation is reduced by an AVC system
- Comparison of the AVC systems with gramian observability optimized sensors or sound power optimized sensors to an ASAC system
- Experimental validation of the effectiveness of the sound power reduction of the AVC systems with optimized error sensors

This paper is structured as follows: First, the experimental set-up and the measurement of the structural model are described. Afterwards, the optimization method used in this paper is presented, and, finally the simulation and the experimental results are presented and discussed.

2. STRUCTURAL OPTIMISATION MODEL

For the error sensor optimization an experimentally identified state-space model of the plate structure and the electrical components is measured. It is also possible to generate a numerical model via finite elements. However, by using an experimental identification all digital signal processing (DSP) and analogue devices (amplifier, anti-aliasing and smoothing filters) are included in the system identification. The experiments are conducted on an aluminum plate ([800x600x3] mm^3) clamped on its four corners

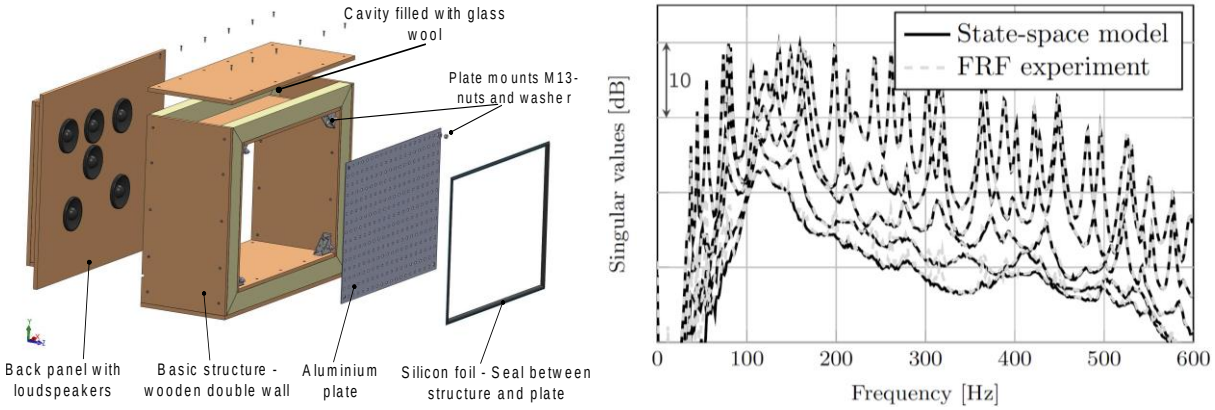

Figure 1: Sketch of the test bed (left) and singular values of the identified and experimental models (right)

with an offset of 35mm in x- and y-directions. At these points, the plate is clamped between two M8 nuts, which are blocked with a torque of 15Nm. A picture of the test-bed is presented in Figure 1.

Five inertial actuators are placed priori due to modal controllability. This type of actuator applies a dynamic force on its host structure through a moving mass excited by a magnetic field (Type VISATON EXS 45). The positions of these inertial exciters are fixed and are not changed during the experiments. In a first step, a basic discrete state-space model with a sampling frequency of 1200 Hz is measured with a coarse sensor grid. Therefore, 10 accelerometers are placed empirically over the plate. For identification the inertial actuators are driven by uncorrelated band-limited white noise signals and the 10 accelerometer signals are measured simultaneously. The input-output time series are post processed with a sub-space based identification algorithm. Thus a 5 input 10 output discrete stable state-space with 500 states is identified [Katayama, 2005].

In the next step, the actuators are driven once again with uncorrelated band-limited white noise signals and a fine regular sensor grid is measured with a laser scanning Doppler vibrometer (LSV). Due to the LSV measurements a frequency response function (FRF) matrix from 5 inputs (inertial exciters) to 300 outputs (surface velocities) has been generated.

In the last step the basic state-space model is used to estimate the FRF matrix. This is done by a curve fitting, so that the generalized state-space model has 5 inputs and 300 outputs. These 300 outputs are the potential error sensor locations which could be used by the optimization. In order to approve the accuracy of the identified and generalized state space model the Hankel singular values of the state-space model and the FRF matrix can be compared. Figure 1 shows a sufficiently accurate state-space model in the frequency range of 50 to 600 Hz. It could be stated that the identified and extended model is sufficient for the optimization. The transfer path from the disturbance actuator (D) to the 300 sensor points is the primary (disturbance) path and the actuators (A1-A4) are used as secondary actuators. A picture of the actuator placement, the sensor grid, and the 10 empirically placed accelerometers is presented in Figure 2.

In order to avoid performance limitations of the control systems due to causality the disturbance path is additionally delayed by 20 samples. This assumption is used throughout the paper.

3. OPTIMIZATION PROCESS

A flowchart of the complete optimization process is given in Figure 2. In the presented studies a genetic optimization is used to optimize the sensor locations. A short description is given in the first subsection. Two different methods to calculate the fitness of each genetic individual was implemented. Therefore, the causal controller used in the proposed method and the classical approach uses gramian observability are described in the following subsections. Finally, the calculation of the sound power due to the radiation resistance matrix (RRM) and the calculation of the ASAC system are described.

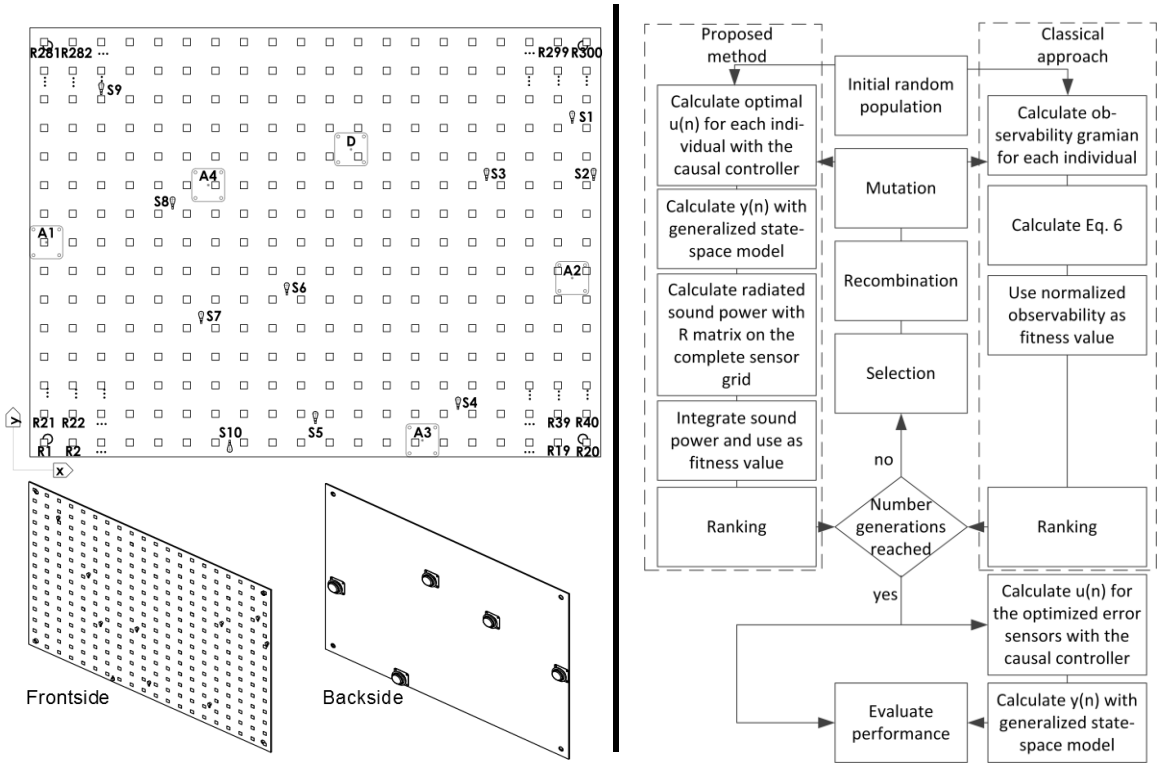

Figure 2: Sensor and actuator positions (left) and optimization flow chart of the two compared sensor placements (right)

3.1 Genetic optimization

In case of sensor placement genetic optimization is often used as a stochastic search technique, since suboptimal solutions can be already found after a few optimization cycles[24]. The different steps of the genetic optimization can be seen in Figure 2. The genetic optimization is based on the evaluation of a fitness function that characterizes the performance of each individual (sensor configuration) in only one scalar. This scalar is called the fitness and is either determined by the radiated sound power of a plate controlled with an AVC system or by a gramian observability metric. The L error sensor positions which are necessary to calculate the AVC system or the gramian observability are determined by the genetic algorithm. For the optimization L of 300 sensors, where $L \ll 300$, are coded into one genetic string. A crossover operator with $L-1$ splitting points is used for recombination because of the discrete error sensor locations.

Furthermore, a number of 160 genetic individuals are used in the randomly generated initial population and it is proved that each sensor candidate location is taken at least one time otherwise a new randomly initial population is generated. These initial population guarantees that each sensor can be selected for a recombination. Further information's of the genetic optimization are summarized in Table 1. Detailed information's about genetic algorithms can be found in the book of Pohlheim[24].

3.2 Causal control

The proposed method uses a causal controller to calculate the optimal actuator voltages for the specified $4 \times L$ AVC system, which is excited by an uncorrelated broadband noise form 50 Hz to 600 Hz applied by the disturbance shaker (D). In order to show the calculation of the optimal actuators signals a very short introduction in the calculation of a MIMO feedforward controller is presented here, for further details see[5]. The cost function of the feedforward controller is given in Eq. 1

$$J = E[\boldsymbol{e}^T(n)\boldsymbol{e}(n)], \tag{1}$$

where $E[\cdot]$ is the expectation error, which can be calculated by averaging over time for ergodic and stationary signals[5]. The vector $\boldsymbol{e}(n)$ describes the L error signals and n is the discrete time. The error signal vector can be expressed as

$$\boldsymbol{e}(n) = [e_1(n) \cdots e_L(n)]^T \tag{2}$$

The error signal is a superposition of L disturbance signals $\boldsymbol{d}(n)$ and L secondary path signals $\boldsymbol{y}(n)$

$$\boldsymbol{e}(n) = \boldsymbol{d}(n) + \boldsymbol{y}(n), \tag{3}$$

where $\boldsymbol{y}(n)$ can be calculated by filtering the four actuator signals $\boldsymbol{u}(n)$ through the $4 \times L$ secondary path state-space model. The optimal actuator signals can be calculated by

$$u(n) = \sum_{i=0}^{I-1} \boldsymbol{W}_i \boldsymbol{x}(n-i), \tag{4}$$

where $\boldsymbol{W}_i$ is the $M \times K$ matrix of the i-th optimal filter coefficients, $\boldsymbol{x}(n)$ is the vector of reference signals, and I is the length of the optimal FIR filter. The optimal filter coefficients can be calculated by using filtered reference signals like it is described in[5]. It is important to notice that these actuator signals are only optimal in reducing the flexural vibrations at the L error sensors. In order to guarantee a limited actuator voltage of maximum 3 Volts the method proposed by Elliott[5] is used where a noise added to the autocorrelation matrix to limit the actuator voltages.

The actuator signals $\boldsymbol{u}(n)$ together with the generalized plant model are further used to calculate the sound radiation of the AVC system.

Table 1: Genetic optimization parameters

Property	**Value**	**Property**	**Value**
Generations	50	Recombination	Crossover
Islands	4	Selection	Stocastic universal sampling
Individuals per island	40	Mutation rate	20%
Individuals (all)	160		

3.3 Gramian observability

The gramian observability matrix is calculated with a discrete state-space model[14] defined by the error sensor locations of the genetic optimization:

$$\boldsymbol{W_O} = \sum_{k=0}^{\infty} (\boldsymbol{A}^T)^k \boldsymbol{C}^T \boldsymbol{C} \boldsymbol{A}^k, \tag{5}$$

where A is the dynamic matrix and C is the output matrix of the state-space model. In order to have a scalar fitness value several functions are used in the literature, for example see[16, 25]. According to this references the observability will be calculated by the following formula:

$$J^{-1} = \frac{trace(\boldsymbol{W}_O)}{\sigma(\lambda_i)}, \tag{6}$$

where λ_i are the eigenvalues of $\boldsymbol{W}_O$, and σ means the deviation of the eigenvalues. It has to be mentioned that the reciprocal value is used as the fitness function to provide a minimization problem. For the calculation of the gramian observability no excitation has to be applied because it is only calculated by the $\boldsymbol{A}$ and $\boldsymbol{C}$ matrix of the discrete state-space model. After the optimization of the error sensor positions the defined secondary paths are used to calculate the optimal causal controller. The same broadband excitation is used as for the proposed method. By doing this the overall performance of a MIMO feedforward system with error sensors optimized via gramian observability can be determined.

3.4 Sound radiation

In order to calculate the sound radiation the complete generalized state-space and the optimal actuator signals, calculated for the $4 \times L$ system, are used to calculate the secondary path signals $\boldsymbol{y}(n)$ at each sensor grid point. By summation of the 300 disturbance signals with the 300 secondary signals the residual error signal $\boldsymbol{e}(n)$ can be calculated for all sensor grid points. These error signals are the controlled surface

velocities of the vibrating plate. Yet, the elemental radiator approach, presented in[6] is used to calculate the radiated sound power by

$$P(\omega) = \boldsymbol{v}_e(\omega)^H \boldsymbol{R}(\omega)\boldsymbol{v}_e(\omega), \tag{7}$$

where $\boldsymbol{v}_e$ are the surface velocities, $\boldsymbol{R}$ is the RRM, and ω is the circular frequency. The discrete time error signals at all grid points can be easily transferred to the frequency domain by a discrete Fourier transformation so that Eq. 7 can be used to calculate the radiated sound power. The RRM can be calculated by geometric properties of the plate by

$$\boldsymbol{R}(\omega) = \frac{\omega^2 \rho_0 S_E^2}{4\pi c_0} \begin{bmatrix} 1 & \frac{\sin(kr_{12})}{kr_{12}} & \cdots & \frac{\sin(kr_{1N})}{kr_{1N}} \\ \frac{\sin(kr_{21})}{kr_{21}} & 1 & & \vdots \\ \vdots & & \ddots & \\ \frac{\sin(kr_{N1})}{kr_{N1}} & \cdots & \cdots & 1 \end{bmatrix}, \tag{8}$$

where ρ_0 is the air density, c_0 is speed of sound in air, k is the wave number, r_{ij} is the distance between the elemental radiators i and j, and S_e is the area of one elemental radiator. In addition, the radiation efficiency is considered, which is defined by

$$\sigma(\omega) = \frac{P(\omega)}{\rho_0 c_0 S \langle \overline{v_n^2}(\omega) \rangle}, \tag{9}$$

where $\langle \overline{v_n^2}(\omega) \rangle$ is the normal averaged quadratic surface velocity and S is the overall vibrating surface.

3.5 ASAC system

For the realization of a feedforward ASAC system radiation modes can be used[4]. The frequency dependent radiation modes can be calculated by a singular value decomposition of the RRM[6]

$$\boldsymbol{R}(\omega) = \boldsymbol{Q}^T(\omega)\boldsymbol{\Lambda}(\omega)\boldsymbol{Q}(\omega), \tag{10}$$

where $\boldsymbol{Q}$ is the matrix of the left and right singular vectors, which are equal for the real, symmetric RRM, and $\boldsymbol{\Lambda}$ is the matrix of singular values. By using Eqs. 7 and 10 and assuming that the off-diagonal terms of the singular value matrix are neglect able, the sound power can be rewritten. For brevity, the frequency dependency on the right hand side of Eq.11 is not shown.

$$\begin{aligned} P(\omega) &= \boldsymbol{v}^H \boldsymbol{R} \boldsymbol{v} \\ &= \boldsymbol{v}^H \boldsymbol{Q}^T \boldsymbol{\Lambda} \boldsymbol{Q} \boldsymbol{v} \\ &= \boldsymbol{a}^H \boldsymbol{\Lambda} \boldsymbol{a} \\ &\approx \boldsymbol{a}^H \sqrt{diag(\boldsymbol{\Lambda})} \sqrt{diag(\boldsymbol{\Lambda})} \boldsymbol{a} \\ &= \boldsymbol{z}^H \boldsymbol{z} \end{aligned} \tag{11}$$

In order to realize a real- time applicable system the radiation modal expansion theory can be used[11]. Therefore, the sound power is estimated by a reduced set of fixed radiation modes $\widetilde{\boldsymbol{Q}}$ and a frequency dependent weighting factor $\sqrt{diag\left(\widetilde{\boldsymbol{\Lambda}}(\omega)\right)}$. In this study six radiation modes are used to estimate the radiated sound power. The radiation modes are estimated at a frequency of 300 Hz. Therefore, the radiation mode signals z can be calculated by

$$\tilde{\boldsymbol{z}}(\omega) = \sqrt{diag\left(\widetilde{\boldsymbol{\Lambda}}(\omega)\right)}\, \widetilde{\boldsymbol{Q}} \boldsymbol{v}(\omega)$$

The term $\sqrt{diag\left(\widetilde{\boldsymbol{\Lambda}}(\omega)\right)}\, \widetilde{\boldsymbol{Q}}$ can be modelled as a state-space and implemented in a MIMO feedforward controller. The radiation mode signals can be used as error signals for the causal feedforward controller, like it is described in Eq. 1, and the overall performance of the ASAC system can be calculated.

4. SIMULATION RESULTS

In order to compare the same configurations in the view of a feedforward controller the ASAC system with six radiation modes and the AVC systems with six error sensors are compared. The AVC system optimized with the proposed method (AVC_{PM}), the AVC system optimized with gramian observability (AVC_{GO}), and the ASAC system are analyzed in detail. The optimized sensor placements of both AVC systems are presented in Figure 3. It can be easily seen that the sensor positions are not regular but the placements are quite different.

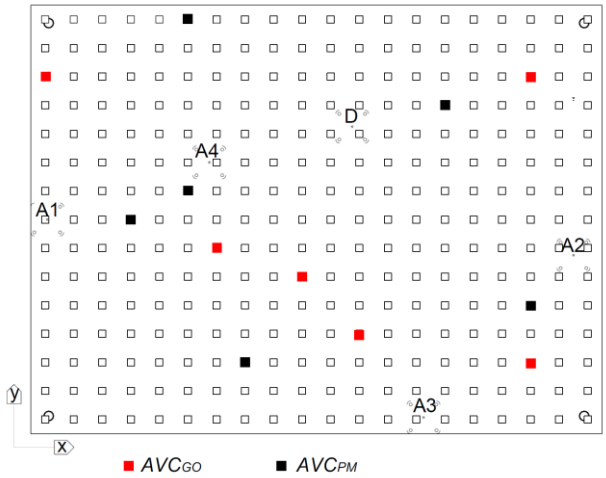

Figure 3: Sensor placements of the two optimizations

The overall performances of the control systems are presented in Table 2. The radiated sound power is calculated by trapezoidal integration of the sound power from 50 Hz to 600 Hz and the global vibration is calculated by averaging the absolute velocities at the 300 grid points followed by trapezoidal integration.
It can be easily seen that the sound power is equally reduced by the AVC_{PM} system and the ASAC system. Surprisingly, the global vibration reduction of the AVC_{PM} system is slightly greater than the global vibration reduction of the AVC_{GO} system. In contrast to the global vibration reduction of both systems, the AVC_{GO} system increases the sound radiation and the AVC_{PM} system decreases the sound power in the range of the ASAC system. Therefore, it could be stated that there is a strong dependence of the sound power reduction and the error sensor positions. This dependence is further explained by the radiation efficiency. Whereas the sensor locations of the AVC_{PM} system lead to slightly reduced but nearly unaffected radiation efficiency compared to the uncontrolled system the radiation efficiency of the AVC_{GO} system is strongly increased.
In order to have a more detailed view the sound power, the global vibration, and the radiation efficiency are presented in the frequency range from 50 to 600 Hz in Figure 4. It can be easily seen that the AVC_{PM} system is more effective than the ASAC in the lower frequency range from 80 Hz to 150 Hz. Above 400 Hz all control systems show equal sound power reductions. The reason for this is that the AVC systems have a lack of observability and controllability because only six error sensors and four actuators are used. In the case of the ASAC system the observability cannot be the explanation but the controllability seems to be insufficient to reduce the sound power above 400 Hz. In fact only four actuators have to influence 38

Table 2: Global performance metrics of the control systems

Metric (Control On – Control Off)	AVC_{GO}	AVC_{PM}	$ASAC$
Sound power [dB]	+5.5	-5.1	-5.1
Global vibration [dB]	-3.0	-3.8	+0.6
Radiation efficiency [-]	+290 %	-30 %	-90%

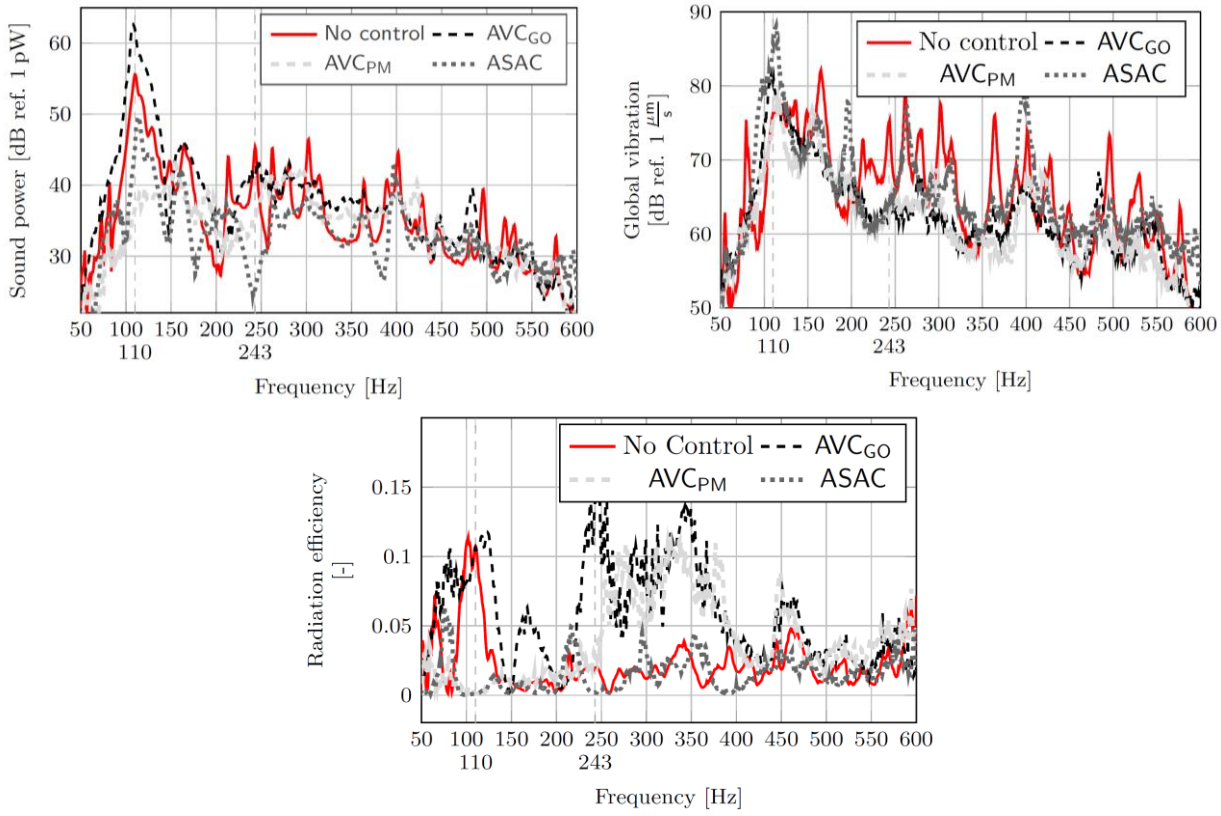

Figure 4: Sound power (top left), global vibration (top right) and radiation efficiency (bottom) of the control systems

mode shapes and as a consequence thereof the sound radiation. In agreement with the sound power reduction the global vibration reduction of the AVC_{PM} system is the highest in the frequency range from 80-150 Hz. But the vibration reduction in this range is not as high and broadband as the sound power reduction. The ASAC system increases the global vibration reduction in the frequency range 75 to 125 Hz about approximately 10 dB. Nevertheless, the ASAC system reduces the sound power in this frequency range due to a restructuring of the ODS.

Also the radiation efficiency of the AVC_{PM} is lower than the radiation efficiency of the ASAC system in the frequency range from 75 Hz up to 150 Hz. Whereas the principle of an ASAC system is to reduce or restructure the efficiently radiating modes the AVC systems influence the sound radiation only indirect with the sensor positions, and by this the lesser radiation efficiency of the AVC_{PM} is a surprising result. Above 225 Hz the radiation efficiency of both AVC systems is dramatically increased. The reason for this can be the use of only six error sensors, whereas the ASAC system has global system information.

In order to have a more detailed view in the working principle of the AVC systems and the ASAC system

Table 3: Performance metrics at the analyzed frequencies

Frequency [Hz]	System	Global vibration reduction [dB]	Sound power reduction [dB]	Radiation efficiency reduction [%]
110	AVC_{GO}	+4.0	+6.3	-1.0
	AVC_{PM}	-1.4	-18.9	-98.8
	ASAC	+9.3	-10.4	-99.2
243	AVC_{GO}	-13.7	-4.3	+605.0
	AVC_{PM}	-12.7	-9.4	+40
	ASAC	-11.6	-20.2	-91

the frequencies at 110 Hz and 243 Hz are analyzed in detail. The ODS at 110 Hz is chosen because the sound power reduction of the AVC_{PM} system is the largest and at 243 Hz all systems show a significant global vibration reduction but a different sound power reduction. It has to be noticed that the frequency of 110 Hz is an off- resonance frequency. The absolute values of the ODS and the real part of the intensity are presented in Fig. 5.

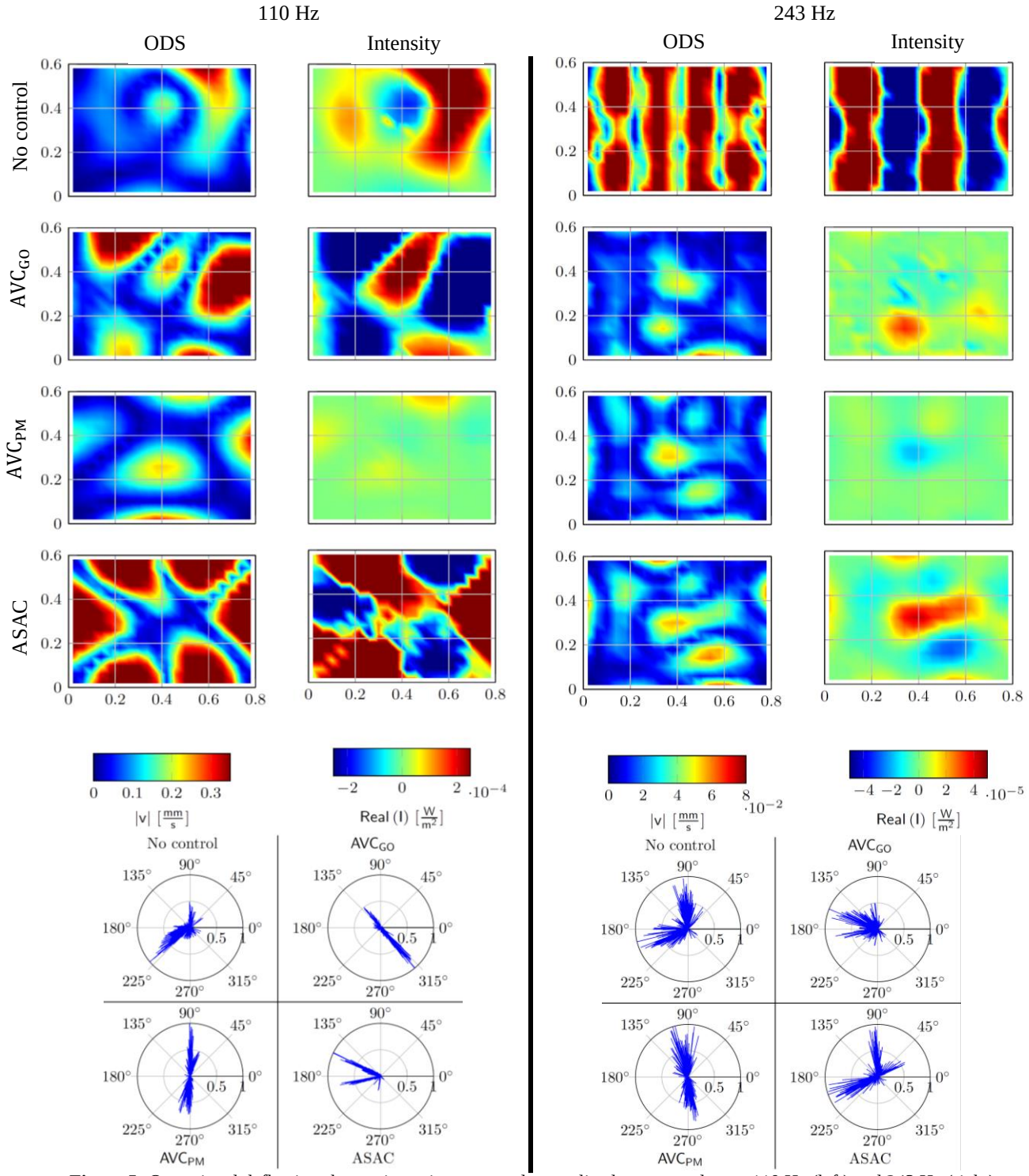

Figure 5: Operational deflection shapes, intensity maps and normalized compass plots at 110 Hz (left) and 243 Hz (right)

It can be seen that all control systems rearrange the structural vibration. The global vibration reduction and sound power reductions are listed in Table 3. At 110 Hz the global vibration is only slightly reduced by the AVC_{PM} system and amplified by the AVC_{GO} and ASAC systems. In contrast to that, the radiated sound power is decreased by the ASAC and AVC_{PM} systems and increased by the AVC_{GO} system. The ASAC system rearranges the ODS such that the negative and positive intensity areas are nearly equal. That supports the acoustic short circuit effect. The distribution of the complex vectors shows not a 180° phase shift, which means that the structure does not vibrate in anti-phase, see Fig.5. The AVC_{GO} system shows no equilibrium between the negative and positive intensity areas. The acoustic short circuit effect cannot be very effective. The complex vectors also show no equilibrium in the amplitudes but they show clearly an anti-phase vibration because the vectors are shifted about 180°. The AVC_{PM} system shows also an anti-phase vibration, but the amplitudes are more homogeneous. This leads to very small intensities all over the plate.
At the resonant frequency of 243 Hz all control systems achieves a comparable global vibration reduction of 12-14 dB. Also the radiated sound power is reduced by all control systems but with a wider scattering of 4-20 dB. The AVC_{GO} shows the largest vibration reduction but there is no anti-phase distribution, like it is shown in Fig 5. Nearly, all complex vectors are in one half plane of the polar plot. Therefore, the acoustic short circuit effect cannot be as effective as in an anti-phase vibration. This can be also seen in the intensity plot on the right side of Fig. 5. The anti-phase intensity regions of the no control case are shifted mainly into two positive intensity dots, which radiate the sound efficiently.
The ODS's of the ASAC and the AVC_{PM} systems seem to be quite equal, whereas the maximum vibration amplitudes of the ASAC system are a bit larger. In contrast, the compass plots of the complex vibration vectors are quite different. The AVC_{PM} system again shows an anti-phase vibration, whereas the ASAC system shows a wider spread of the phases. But the phase spread in the velocities of the ASAC system results in a intensity distribution that is anti-phase and shows a 10 dB higher sound power reduction than the more homogeneously intensity distribution of the AVC_{PM} system.
It can be summarized that the proposed method finds optimal error sensor locations that reduce the global vibration, reduce the sound power and, do not increase the radiation efficiency. Additionally, the sound power reduction of the proposed method is comparable to the ASAC system but is mainly limited to a smaller frequency range. In contrast, the ASAC system increases the global vibration reduction and decrease the radiated sound power in a wider frequency range. The increased global vibration reduction can be critical for some applications[10]. Therefore, a feedforward system with error sensors optimized with the proposed method is applicable for sound power reduction problems where the global vibration reduction has to be simultaneously reduced.

5. EXPERIMENATL VALIDATION

In order to validate the proposed error sensor optimization method a 4 actuator 10 sensor system is investigated. The ASAC system is not realized in the experiments due to the very large number of sensors which have to be used. The AVC_{PM} system is compared to the AVC_{GO} system. The measured sound power reductions are presented in Figure 6.
It can be easily seen that the experiments are not as effective as the simulation prediction. This is mainly due to a complete reassembly of the test stand, where the plate and the silicon foil removed from the test stand and build in again after the optimizations were completed. This reassembly results in small shifts in the resonance frequency and small damping variations because the silicon foil is glued with two sided tape to the aluminum plate. Nevertheless, the simulated tendencies can be easily measured.
The sound power reduction of the AVC_{PM} can be validated whereas the neglect able reduction of the AVC_{GO} system can be also measured. Finally, it can be stated that the simulated results can be experimentally validated if the reassembly of the test bed is considered. The experiments show that the robustness of the sensor placement against model uncertainties has to be also studied.

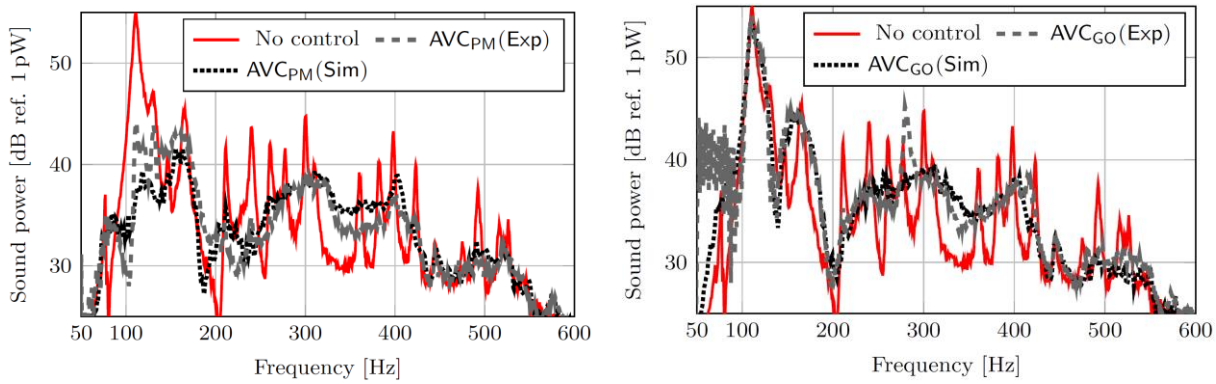

Figure 6: Measured and simulated sound power for the AVC_{PM} system (left) and the AVC_{GO} system (right)

6. CONCLUSIONS

This paper examines the error sensor placement for an active vibration feedforward control system. The proposed method optimizes the multiple error sensor positions for an AVC system with regard to the radiated sound power. It uses the local vibration reduction of an AVC system and the resulting rearrangement of the ODS's to indirectly influence the radiated sound power. Afterwards the proposed method is compared to a gramian observability based error sensor placement for an AVC system and an ASAC system. The optimization model is experimentally identified. A state-space model with five actuators and 300 possible error sensor locations is measured and provides the disturbance path and the secondary paths for the AVC systems which error sensor positions optimized by a genetic algorithm.
First of all, AVC systems with six error sensors are optimized and their performance is compared to an ASAC system which is presented as superior for sound power reduction in the literature[6]. The comparison is made with six error sensors because the ASAC system uses six radiation modes to estimate the radiated sound power, which results in the same control problem for the feedforward controller. In the simulations the AVC_{PM} shows a 5.1 dB reduction in sound power which is equal to the performance of the ASAC system.
An advantage of the AVC_{PM} system is the simultaneous reduction of the global vibration of 3.8 dB and the sound power of 5.1 dB whereas the ASAC system results in an amplification of the global vibration of 0.6 dB and a reduction in sound power of 5.1 dB over the frequency range from 50 Hz to 600 Hz. Like it is presented in the literature an AVC system which is optimized for vibration reduction can result in an amplified sound power. The AVC_{GO} system with error sensors optimized with gramian observability shows exactly this behavior. A reduced global vibration reduction of 3 dB leads to an amplification in sound power of 5.5 dB. Finally, it can be said that the proposed method is superior in reducing sound power compared to the classical gramian based error sensor placement. Compared to an ASAC system the sound power reduction is equal and the global vibration is also reduced by the proposed method. The simulated sound power and global vibration reductions are also experimentally validated on a 4 actuator and 10 error sensor system.

REFERENCES

1. Bachmann, F. ; Bergamini, A.E. ; Ermanni, P.: Optimum piezoelectric patch positioning: A strain energy based finite element approach. In: Journal of Intelligent Material Systems and Structures 23 (2012), Nr. 14, p. 1575{1591
2. Bianchi, E., Gardonio, P., Elliott, S.J., "Smart panel with multiple decentralized units for the control of sound transmission. Part III: control system implementation." *Journal of Sound and Vibration*, Vol. 274, Nr. 1, 2004, pp. 215-232.

3. Clark, R. L., Fuller, C. R., "Optimal placement of piezoelectric actuators and polyvinylidene fluoride error sensors in active structural acoustic control approaches", *Journal of the Acoustical Society of America*, Vol. 3, 1992, pp. 1521- 1533
4. Elliott, S.J., Johnson, M.E., "Radiation modes and the active control of sound power", *Journal of the Acoustical Society of America*, Vol. 94, Nr. 4, 1993, pp. 2194-2204
5. Elliott, S. J., "Signal processing for active control", Academic Press, 2001
6. Fahy, F. J., Gardonio, P., "Sound and structural vibration: radiation, transmission and response", Academic press, 2007
7. Frecker, M. I., "Recent Advances in Optimization of Smart Structures and Actuators", *Journal of Intelligent Material Systems and Structures*, Vol. 14, 2003, pp. 207-216
8. Gardonio, P., Bianchi, E., Elliott, S.J., "Smart panel with multiple decentralized units for the control of sound transmission. Part I: theoretical predictions", *Journal of Sound and Vibration*, Vol. 274, Nr. 1, 2004, pp. 163-192.
9. Gardonio, P., Bianchi, E., Elliott, S.J., "Smart panel with multiple decentralized units for the control of sound transmission. Part II: design of the decentralized control units", *Journal of Sound and Vibration*, Vol. 274, Nr. 1, 2004, pp. 193-213.
10. Gardonio, P., "Review of active techniques for aerospace vibro-acoustic control", *Journal of Aircraft*, Vol. 39, Nr. 2, 2002, pp. 206-214
11. Gibbs, G.P., Clark, R.L., Cox, D.E., Vipperman, J.S., "Radiation modal expansion: Application to active structural acoustic control" *Journal of the Acoustical Society of America*, Vol. 107, 2000
12. Gupta, V., Sharma, M., Thakur, N., "Optimization Criteria for Optimal Placement of Piezoelectric Sensors and Actuators on a Smart Structure: A Technical Review", *Journal of Intelligent Material Systems and Structures*, Vol. 21, 2010, pp. 1227-1243
13. Haase, T., Algermissen, S., Unruh, O., Misol, M., "Experiments on Active Control of Counter-Rotating Open Rotor Interior Noise", *Acta Acustica united with Acustica*, Vol. 100, Nr. 3, 2014, pp. 448-457
14. Kailath, T., "Linear systems", Prentice-Hall, 1980
15. Katayama, T., "Subspace methods for system identification", Springer, 2005
16. Leleu, S., Abou-Kandil, H., Bonnassieux, Y., "Piezoelectric actuators and sensors location for active control of flexible structures", *IEEE Transactions on Instrumentation and Measurement*, Vol. 50, Nr. 6, 2001, pp. 1577-1582
17. Li, D.S., Cheng, L, "The design of synthesized structural acoustic sensors for active control of interior noise with experimental validation", *Journal of Sound and Vibration*, Vol. 329, Nr. 2, 2010, pp. 123-139
18. Liang, C., Sun, F.P., Rogers, C.A., "Determination of design of optimal actuator location and configuration based on actuator power factor", *Journal of Intelligent Material Systems and Structures*, Vol. 6, Nr. 4, 1995, pp. 456-464
19. Minkoff, J., "The operation of multichannel feedforward adaptive systems", *IEEE Transactions on Signal Processing*, Vol. 45, Nr. 12, 1997, pp. 2993-3005
20. Misol, M., Algermissen, S., Monner, H.P, "Experimental investigation of different active noise control concepts applied to a passenger car equipped with an active windshield", *Journal of Sound and Vibration*, 2012
21. Nijhuis, M. O., "Analysis tools for the design of Active Structural Acoustic Control Systems", *University of Twente*, Enschede, Ph.D. thesis, 2003
22. Nijhuis, M. O., Boer, A. de, "Optimization strategy for Actuator and Sensor placement in active structural acoustic control", *Proceedings of ACTIVE*, 2002
23. Padula, S. L., Palumbo, D. L., Kincaid, R. K., "Optimal Sensor/Actuator Locations for Active Structural Acoustic control", *39th AIAA/ASME/ASCE/AHS/ASC Structures, Structural Dynamics, and Materials Conference*, 1998
24. Pohlheim, H., „Evolutionäre Algorithmen", Springer, 1999
25. Pulthasthan, S., Pota, H. R., "The optimal placement of actuator and sensor for active noise control of sound-structure interaction systems", *Smart Materials and Structures*, Vol. 17, Nr. 3, 2008
26. Wang, B.-T., "Optimal placement of microphones and piezoelectric transducer actuators for far-field sound radiation control", *Journal of the Acoustical Society of America*, Vol. 5, 199), pp. 2975-2984